Proceedings of
ASME TURBOEXPO 2000
May 8-11, 2000, Munich Germany

2000-GT-416

NON-UNIFORM FLOW IN A COMPRESSOR DUE TO ASYMMETRIC TIP CLEARANCE

Seung Jin Song
&
Seung Ho Cho
School of Mechanical and Aerospace Engineering
Seoul National University
Seoul 151-742, Korea
Tel: 82-2-880-1667
Fax: 82-2-883-0179
Email: sjsong@snu.ac.kr

ABSTRACT

This paper presents an analytical study of flow redistribution in a compressor stage due to asymmetric tip clearance distribution. The entire stage is modeled as an actuator disc, and it is assumed that upstream and downstream flow fields are determined by the local tip clearance. The flow is assumed to be inviscid and incompressible. First, an axisymmetric flow model is used to connect upstream and downstream flows. Second, a linear perturbation approximation is used for non-axisymmetric analysis in which each flow variable is assumed to consist of a mean (axisymmetric value) plus a small perturbation (asymmetric value). Thus, the perturbations in velocity and pressure induced by the tip clearance asymmetry are predicted. Furthermore, rotordynamic effects of such flow non-uniformity are examined as well.

Nomenclature

SYMBOL DEFINITION

B	Bernoulli constant, m^2/s^2
C	absolute flow velocity, m/s
c	axial blade chord, m
C_l'	lift coefficient per unit span, [1]
C_p	pressure coefficient, [1]
e	magnitude of rotor offset, m
E_i	eigenvector for downstream perturbations
F_X	lateral force in the direction of the offset, N
F_Y	lateral force perpendicular to the direction of the offset, N
H	annulus height, m
H_b	rotor blade span, m
$\hat{K}_i$	complex amplitude of flow perturbations
L	axial rotor hub thickness, m
$\dot{m}$	mass flux, kg/s
P	pressure, Pa
Q	strength of shear layer, m^2/s^2
q	nondimensional vorticity strength; local mass flux, [1]
R	mean compressor radius, m
s	blade pitch, m
t	radial tip clearance, m
$U = \omega R$	compressor rotational speed at the mean radius, m/s
W	relative velocity, m/s
X	direction along the rotor offset
x	axial direction
Y	direction perpendicular to rotor offset
y	tangential direction
z	radial direction
ZW	Zweifel coefficient, [1]

Greek Symbols

α	absolute flow angle, deg; eigenvalue
α_X	direct excitation force coefficient, [1]
α_Y	cross excitation force coefficient, [1]
β	relative flow angle, deg
Δ	thickness of underturned layer downstream of actuator disc, m
ϕ	upstream velocity potential
$\Phi = C_x / U$	flow coefficient, [1]
λ	nondimensional mass fraction of underturned flow, [1]
θ	azimuthal angle measured in the direction of rotation from the minimum gap location, deg; angle of underturning relative to passage flow, deg
ρ	density, kg/m^3
ω	angular velocity of rotor shaft rotation, s^{-1}
ψ	meridional stream function; work coefficient, [1]

Subscripts

D	design value
G	gap
m	mean
p	indicates effect due to nonuniform pressure
ps	pressure side
R	rotor
S	stator
ss	suction side
t	stagnation condition
wd	indicates effect due to variation of torque or tangential force
0-	near upstream of the actuator disc on the radius scale
0+	near downstream of the actuator disc on the radius scale
$-\infty$	far upstream on the blade scale
0	IGV inlet on the blade scale
1	rotor inlet on the blade scale
2	stator inlet on the blade scale
3	stator outlet on the blade scale
$+\infty$	far downstream on the blade scale
$\perp$	meridional component

Superscripts

a	the part of downstream flow associated with the rotor tip gap
b	the part of downstream flow which has crossed the bladed part of compressor
c	the part of downstream flow associated with the stator tip gap
'	non-axisymmetric perturbation
-	azimuthal mean, or axisymmetric value
^	complex amplitude

1. Introduction

Non-axisymmetric tip clearance degrades both aerodynamic and structural performance of turbomachinery, and the tip clearance asymmetry can have many causes such as rotor shaft bending, whirling, casing asymmetry, and deformation of components. The effects of rotor tip clearance asymmetry on turbine rotors were initially suggested by Thomas (1958) and Alford (1965). They suggested that the variation in efficiency with local clearance would lead to a destabilizing forward whirl-inducing force. This suggestion was experimentally verified by Urlichs (1983), Wohlrab (1983) and Martinez-Sanchez et al. (1995). Martinez-Sanchez et al. also identified non-axisymmetric pressure acting radially on the turbine hub as a second source of forcing mechanism in addition to the non-axisymmetric torque initially hypothesized by Thomas and Alford. Analytically, Song & Martinez-Sanchez (1997a, 1997b) developed an actuator disc model which could accurately predict both non-axiymmetric torque and pressure effects in turbines.

To examine the effects of compressor tip clearance asymmetry, Horlock & Greitzer (1983) and Colding-Jorgensen (1992) formulated actuator disc models. Also, Ehrich (1993) and Graf et al. (1998) developed parallel compressor models. All of the models above require compressor performance data as inputs. Therefore, Park (1998) developed an analytical model to predict the effects of non-axisymmetric rotor tip clearance in a single stage compressor without empiricism. All of the models predict a backward whirl-inducing force due to torque asymmetry at the design point. In addition, Park (1998) predicts a forward whirl-inducing cross force due to pressure asymmetry.

Until now, the attention has been focused only on the effects of rotor tip clearance asymmetry. However, real machines operate with tip clearances in both rotors and stators. Furthermore, the results from a recent experiment conducted in the Low Speed Research Compressor (LSRC) at GE (Storace et al., 2000) strongly suggest contributions from the stator tip clearance asymmetry.

Therefore, this investigation aims to understand the flow fields and rotordynamic effects in compressors caused by non-axisymmetry in both rotor and stator tip clearances. The scope of current investigation is limited to the effects of static tip clearance asymmetry in a single stage compressor. An analytical actuator disc approach is used in this investigation.

2. Analytical Model

The modeling approach is similar to the approach of Song & Martinez-Sanchez (1997a, 1997b). A two-step process is used to solve for the flow through a compressor stage. First step is an axisymmetric, two-dimensional, meridional plane analysis, or the blade scale analysis. This analysis examines radial redistribution of flow due to axisymmetric rotor and stator tip clearances. The top part of Figure 1 shows the blade scale view of the stage. Due to tip clearance flows, the radially uniform upstream flow is assumed to split into three streams – "a", "b", and "c" – upon going through the inlet guide vane (IGV), rotor, and stator. Streams "a" and "c" are associated with the rotor and stator tip clearances, respectively. Stream "b" is the rest of the passage flow which has passed through the bladed part of both rotor and stator rows.

Second step is a non-axisymmetric, two-dimensional, radial plane analysis. The tip clearance asymmetry is a non-uniformity with a length scale on the order of the turbine radius. Therefore, this latter analysis is referred to as the radius scale analysis. It examines the flow redistribution in the azimuthal direction caused by non-axisymmetric tip clearance distribution. This view, with a non-axisymmetric tip clearance distribution, is shown schematically in the bottom part of Figure 1. This analysis is a small perturbation (tip clearance asymmetry) analysis about the mean (axisymmetric) solution provided by the blade scale analysis. Therefore, the results from the blade scale analysis are perturbed to provide connecting conditions across the actuator disc.

The actuator disc in this study consists of an inlet guide vane (IGV) row, a rotor blade row, and a stator blade row. The IGV has full span blades while rotor and stator have partial span blades. Axial, tangential, and radial directions are denoted by x, y, and z, respectively. On the blade scale, $-\infty$ refers to a location far upstream of the IGV. Near upstream of the IGV is referred to as Station 0. Inlet to the rotor is referred to as Station 1, and the rotor exit is called Station 2. Downstream of the stator row is called Station 3. Far downstream is referred to as $+\infty$. On the radius scale x=0- and x=0+ are equivalent to $-\infty$ and $+\infty$ at the blade scale, respectively. The compressor's rotational speed, absolute velocity, and relative

velocity are U, C, and W, respectively. α is the absolute flow angle, and β is the relative flow angle.

The model assumes an inviscid, incompressible flow. The compressor geometry is assumed to be two dimensional at the mean radius values. Also, the flow is assumed to follow the blades perfectly. Thus, effects such as blockage and deviation are not accounted for in this model.

2. 1. Tip Scale Analysis

Martinez-Sanchez (1990) developed an inviscid tip clearance flow model (Figure 2) whose predictions agreed with the theory and data of Chen (1991) (Song & Martinez-Sanchez, 1997a). The tip clearance flow ("jet" in Figure 2) is modeled as a jet driven by the pressure difference between the pressure and suction sides. This jet then collides with an equal amount of passage ("pass" in Figure 2) flow before rolling up into a vortex. Finally, this tip vortex forms a layer which is underturned relative to the passage flow. For example, at the rotor exit, Stream "b" is the passage flow and Stream "a" is the underturned flow due to the rotor tip clearance.

The turbine tip clearance flow model has been modified for compressors (Roh, 1997), and the compressor tip clearance flow model is shown schematically in Figure 3. The flow velocities on suction and pressure sides are obtained from the Beruoulli equation

$$W_{ps} = \sqrt{W_1^2 - 2\frac{p_{ps} - p_1}{\rho}} \tag{1}$$

$$W_{ss} = \sqrt{W_1^2 - 2\frac{p_{ss} - p_1}{\rho}} \tag{2}$$

where 1 refers to the rotor inlet condition. Also,

$$W_G = \sqrt{2\frac{p_{ps} - p_{ss}}{\rho}} \tag{3}$$

Since the flow is assumed to be inviscid, the two streams ("jet" and "ss" in Figure 3) which collide have same total pressure, temperature, and also equal static pressures along their contact line. Therefore, these two streams must have equal velocity magnitudes, and the line OP bisects the angle made by $\vec{w}_{jet}$ and $\vec{w}_{ss}$ (Figure 3),Then

$$\tan 2\theta = \frac{W_G}{W_{ps}} = \sqrt{\frac{C_{p_{ps}} - C_{p_{ss}}}{1 - C_{p_{ps}}}} \tag{4}$$

where $C_p = \frac{p - p_1}{\rho W_1^2/2}$. Notice that $C_l' = C_{p_{ps}} - C_{p_{ss}}$, and it can be shown that the degree of underturning of the vortex relative to the passage flow can be obtained as

$$\theta = \cos^{-1}\sqrt{\frac{4}{4 + C_l'}} \tag{5}$$

where

$$C_l' = ZW\left(\frac{\cos\beta_1}{\cos\beta_2}\right)^2 \tag{6}$$

and ZW refers to the Zweifel coefficient

$$ZW = 2\frac{(s/c)}{(H/c)}\cos^2\beta_2(\tan\beta_1 - \tan\beta_2) \tag{7}$$

2. 2. Blade Scale Analysis

The azimuthal momentum equation for the flow is

$$\vec{C}_\perp \cdot \nabla C_y = 0 \tag{8}$$

where $\vec{C}_\perp = \vec{i}C_x + \vec{k}C_z$ is the meridional velocity decoupled from the azimuthal velocity. The azimuthal component of vorticity $\omega_y = \frac{\partial C_x}{\partial z} - \frac{\partial C_z}{\partial x}$ can be described in terms of the stream function Ψ as

$$\omega_y(\Psi) = \nabla_\perp^2\Psi \quad (\nabla_\perp^2 = \frac{\partial^2}{\partial x^2} + \frac{\partial^2}{\partial z^2}) \tag{9}$$

The upstream flow is irrotational(ω_y=0). Therefore, Ψ obeys the Laplace equation. Downstream, ω_y is concentrated at the interfaces between Streams "a", "b", and "c" (Q_R & Q_S in Figure 1).

Defining the Bernoulli constant as $B_\perp = \frac{P}{\rho} + \frac{1}{2}C_\perp^2$,

$$\omega_y = \frac{dB_\perp}{d\Psi} \tag{10}$$

From the definition of $B_\perp$, with the continuity constraint and the assumption of spanwise uniform blading,

$$B_{\perp 3} - B_{\perp 1} = \frac{P_3 - P_1}{\rho} \tag{11}$$

Upstream of the stage, $dB_{\perp 1}/d\Psi = 0$ due to the flow's irrotationality. Then, Eq.(10) becomes

$$\omega_{y3} = \frac{dB_{\perp 3}}{d\Psi} = \frac{d(B_{\perp 3} - B_{\perp 1})}{d\Psi} = \frac{d}{d\Psi}(\frac{P_3 - P_1}{\rho}) \tag{12}$$

and ω_1 can be determined from the static enthalpy addition $(P_3 - P_1)/\rho$ by the compressor. From Euler's equation, the static enthalpy rise is given by

$$(\frac{P_3 - P_1}{\rho}) = U(C_{y2} - C_{y1}) - \frac{1}{2}(C_3^2 - C_1^2) \quad (13)$$

At the IGV exit, tangential velocity is given as

$$C_{y1} = C_{x1} \tan\alpha_1 \quad (14)$$

At the rotor exit, the flow has split into two streams. For the bladed stream (Stream "b"), the tangential velocities at the rotor exit (2) and stator exit (3) are

$$C_{y2}^b = U - C_{x2}^b \tan\beta_2 \quad (15)$$

$$C_{y3}^b = C_{x3}^b \tan\alpha_3 \quad (16)$$

Thus, the pressure rise for Stream "b" is

$$(\frac{P_3 - P_1}{\rho})^b = U(C_{y2}^b - C_{y1}) - \frac{1}{2}[C_{x3}^{b2} + C_{y3}^{b2} - (C_{x1}^2 + C_{y1}^2)] \quad (17)$$

For Stream "a", the tip scale analysis predicts its rotor exit azimuthal velocity to be

$$C_{y2}^a = U - C_{x2}^a \frac{\cos(\theta_R)\sin(\beta_m + \theta_R)}{\cos(\beta_m)} \quad (18)$$

where β_m is the mean flow angle through the rotor and θ_R is the underturning of the Stream "a" relative to the Stream "b". Also at the stator exit,

$$C_{y3}^a = C_3^a \tan\alpha_3 \quad (19)$$

Similarly, for Stream "c", the tangential velocities at the rotor exit (2) and stator exit (3) are given as

$$C_{y2}^c = C_{y2}^b \quad (20)$$

$$C_{y3}^c = C_{x3}^c \frac{\cos\theta_S \sin(\alpha_m + \theta_S)}{\cos\alpha_m} \quad (21)$$

Thus, the pressure rise for Streams "a" and "c" are

$$(\frac{P_3 - P_1}{\rho})^a = U(C_{y2}^a - C_{y1}) - \frac{1}{2}(C_{x3}^{a2} + C_{y3}^{a2}) - (C_{x2}^a \frac{\sin(\theta_R)}{\cos(\beta_m)})^2 + (C_{x1}^2 + C_{y1}^2) \quad (22)$$

and

$$(\frac{P_3 - P_1}{\rho})^c = U(C_{y2}^b - C_{y1}) - \frac{1}{2}(C_{x3}^{c2} + C_{y3}^{c2}) - (C_{x3}^c \frac{\sin(\theta_S)}{\cos(\alpha_m)})^2 + (C_{x1}^2 + C_{y1}^2) \quad (23)$$

The third terms on the right side of Eqs. (22) and (23) are the kinetic energy dissipated when the leakage through the tip gaps collides with the passage flow before rolling up into vortices.

To focus on the tip clearance effects, the coordinate system is transformed to the streamline coordinate from the z coordinate. Then, the equation for Ψ becomes

Upstream (x<0) $\nabla_\perp^2 \Psi = 0$ (24)

Downstream(x>0)

$$\nabla_\perp^2 \Psi = Q_R \delta(\Psi - \Psi_{rotortip}) + Q_S \delta(\Psi - \Psi_{statortip}) \quad (25)$$

where $Q = \int^j \omega_y d\Psi = B_{\perp 3}^j - B_{\perp 3}^i$ is the strength of the ω_y between streams i and j, and δ is Dirac's delta function.

The boundary conditions are

$$\Psi(x,0) = 0 \qquad \Psi(x,H) = C_{x0} H$$

$$\Psi(x=0-,z) = C_{x0} z \qquad \frac{\partial \Psi}{\partial x}(x=0+,z) = 0 \quad (26)$$

$$\Psi_1(z) = \Psi_3(z) \qquad \frac{\partial \Psi_1(z)}{\partial z} = \frac{\partial \Psi_3(z)}{\partial z}$$

From the definition of $B_\perp$ and Eqs.(17), (22) and (23), the strengths of vorticity, Q_R and Q_S, in the shear layers (Figure 1) are

$$Q_R = U(C_{y2}^a - C_{y1}) - U(C_{y2}^b - C_{y1}) - \frac{1}{2}(C_{y3}^{a2} + (C_{x2}^a \frac{\sin(\theta_R)}{\cos(\beta_m)})^2 - C_{y3}^{b2}) \quad (27)$$

$$Q_S = U(C_{y2}^b - C_{y1}) - U(C_{y2}^c - C_{y1}) - \frac{1}{2}(C_{y3}^{b2} - (C_{x3}^c \frac{\sin(\theta_S)}{\cos(\alpha_m)})^2 - C_{y3}^{c2}) \quad (28)$$

Subsequently, the velocities at various axial locations can be determined. At the rotor exit, axial velocities for Streams "a" and "b" are

$$C_{x2}^a = C_{x1}(1 + \frac{q_R}{2}(1 - \lambda_R)) \quad (29)$$

$$C_{x2}^b = C_{x1}(1 - \frac{q_R}{2}\lambda_R) \quad (30)$$

where $q_R = Q_R / C_{x1}^2$ and λ_R is the nondimentional mass fraction of Stream "a". Tangential velocities are given in Eqs. (15) and (18).

At the stator exit, the axial velocities are

$$C_{x3}^a = C_{x1}(1 + \frac{q_R}{2}(1-\lambda_R) + \frac{q_S}{2}\lambda_S) \quad (31)$$

$$C_{x3}^b = C_{x1}(1 - \frac{q_R}{2}\lambda_R + \frac{q_S}{2}\lambda_S) \quad (32)$$

$$C_{x3}^c = C_{x1}(1 - \frac{q_S}{2}(1-\lambda_S) - \frac{q_R}{2}\lambda_R) \quad (33)$$

and tangential velocities are given in Eqs. (16), (19), and (21).

Far downstream of the stator, the axial velocities are

$$C_{x+\infty}^a = C_{x1}(1 + q_R(1-\lambda_R) + q_S\lambda_S) \quad (34)$$

$$C_{x+\infty}^b = C_{x1}(1 - q_R\lambda_R + q_S\lambda_S) \quad (35)$$

$$C_{x+\infty}^c = C_{x1}(1 - q_S(1-\lambda_S) - q_R\lambda_R) \quad (36)$$

and tangential velocities are equivalent to those at the stator exit given in Eqs. (16), (19), and (21).

Substituting for velocities in Eqs (27) & (28) yields two quadratic equations for Q_R and Q_S as functions of blade geometry and mass fractions of Streams "a" and "c", λ_R and λ_S.

$$[(1-2\lambda_R)\tan^2\alpha_3](\frac{q_R}{2})^2 + 2[2+\tan^2\alpha_3(1+\frac{\lambda_S q_S}{2})](\frac{q_R}{2}) + [(1+\frac{q_R}{2}(1-\lambda_R))^2(\frac{\sin\theta_R}{\cos\beta_m})^2 + \frac{2}{\Phi}(1+\frac{q_R}{2}(1-\lambda_R))T - \frac{2}{\Phi}(1-\frac{q_R\lambda_R}{2})\tan\beta_2] = 0 \quad (37)$$

where, $T = \dfrac{\cos(\theta_R)\sin(\beta_m + \theta_R)}{\cos(\beta_m)}$

and for the stator

$$[\lambda_S^2(\tan^2\alpha_3 - G_S) - (1-2\lambda_S)G_S](\frac{q_S}{2})^2 + 2[2+(1-\frac{q_R\lambda_R}{2})\{\lambda_S(\tan^2\alpha_3 - G_S) + G_S\}](\frac{q_S}{2}) + (1-\frac{q_R\lambda_R}{2})^2(\tan^2\alpha_3 - G_S) = 0 \quad (38)$$

where $G_S = (\dfrac{\sin(\theta_S)}{\cos(\alpha_m)})^2 + (\dfrac{\cos(\theta_S)\sin(\alpha_m + \theta_S)}{\cos(\alpha_m)})^2$

Next, the mass fractions, λ_R and λ_S, can be determined from the given tip clearances as

$$\lambda_R = \frac{4(t_R/H)}{(1-\frac{q_R}{2}-\frac{q_S}{2}\frac{\lambda_S}{2}) + \sqrt{(1-\frac{q_R}{2}-\frac{q_S}{2}\frac{\lambda_S}{2})^2 - 4\frac{q_R}{2}\frac{t_R}{H}}} \quad (39)$$

and

$$\lambda_S = \frac{4(t_S/H)}{(1+\frac{q_S}{2}+\frac{q_R}{2}\frac{\lambda_R}{2}) + \sqrt{(1+\frac{q_S}{2}+\frac{q_R}{2}\frac{\lambda_R}{2})^2 - 4\frac{q_S}{2}\frac{t_S}{H}}} \quad (40)$$

Thus, from the prescribed tip clearances t_R/H and t_s/H, Eqs. (37)-(40) can be solved for Q_R, Q_S, λ_R, and λ_s.

Far downstream, after the completion of flow readjustment, the thicknesses of Streams "a" and "c" can be determined as

$$\frac{\Delta_R}{H} = \lambda_R[1 - \frac{q_R}{2}(1-\frac{\lambda_R}{2}) - \frac{q_S}{2}\frac{\lambda_S}{2}]\frac{1+\frac{q_R}{2}(1-\lambda_R)+\frac{q_S}{2}\lambda_S}{1+q_R(1-\lambda_R)+q_S\lambda_S} \quad (41)$$

$$\frac{\Delta_S}{H} = \lambda_S[1 + \frac{q_S}{2}(1-\frac{\lambda_S}{2}) + \frac{q_R}{2}\frac{\lambda_R}{2}]\frac{1-\frac{q_S}{2}(1-\lambda_S)-\frac{q_R}{2}\lambda_R}{1-q_S(1-\lambda_S)-q_R\lambda_R} \quad (42)$$

Also, the pressure rise across the compressor stage can be determined as

$$\frac{P_{-\infty} - P_{+\infty}}{\rho} = U(C_{y1} - C_{y2}^b) + \frac{1}{2}C_{x+\infty}^{b\,2} - \frac{1}{2}C_{x-\infty}^{\;2} + \frac{1}{2}C_{y3}^{b\,2} \quad (43)$$

2. 3. Radius Scale Analysis

The rotor offset, e, is assumed to be much smaller than the blade span. Therefore, the tip clearance distribution is given by

$$t = \bar{t} + \mathrm{Re}[\hat{e}e^{i(y/R)}] \quad (44)$$

where $\bar{t}$ is the mean rotor tip gap, and y is the distance from the maximum tip gap in the azimuthal direction (Figure 4).

2. 3. 1. Upstream Flow

The irrotational upstream flow is given by

$$\nabla^2\phi = 0 \quad (45)$$

where ϕ is the velocity potential. Far upstream, $C_x(-\infty) = \bar{C}_{x-\infty}$. Near upstream of the stage at x = 0-, the axial and tangential velocities are

$$C_x(0-, y, t) = \mathrm{Re}[\bar{C}_{x-\infty} + \hat{K}_0 e^{i(y/R)}] \quad (46)$$

$$C_y(x, y, t) = \mathrm{Re}[i\hat{K}_0 e^{x/R + i(y/R)}] \quad (47)$$

where $\hat{K}_0$ is the complex amplitude of axial velocity perturbation as the flow approaches the disc. Therefore, the upstream pressure is given by

$$P(x,y,t) = P(-\infty) - \mathrm{Re}\left[\rho(\overline{C}_{x-\infty})\,\hat{K}_0 e^{x/R+i(y/R)}\right] \qquad (48)$$

2. 3. 2. Downstream Flow

Downstream of the stage, the flow consists of three regions – Streams "a", "b", and "c". The continuity equation for each stream can be written as

$$\frac{\partial \Delta_R}{\partial t} + \frac{\partial(C_x^a \Delta_R)}{\partial x} + \frac{\partial(C_y^a \Delta_R)}{\partial y} = 0 \qquad (49)$$

$$\frac{\partial \Delta_S}{\partial t} + \frac{\partial(C_x^c \Delta_S)}{\partial x} + \frac{\partial(C_y^c \Delta_S)}{\partial y} = 0 \qquad (50)$$

$$\frac{\partial(H-\Delta_R-\Delta_S)}{\partial t} + \frac{\partial(C_x^c(H-\Delta_R-\Delta_S))}{\partial x} + \frac{\partial(C_y^c(H-\Delta_R-\Delta_S))}{\partial y} = 0 \qquad (51)$$

where H is annulus height and Δ_R and Δ_S are given by Eqs. (41) and (42). The momentum equations for the three streams can be written as

$$\frac{\partial \vec{C}^{a,b,c}}{\partial t} + (\vec{C}^{a,b,c} \cdot \nabla)\vec{C}^{a,b,c} + \frac{1}{\rho}\nabla P = 0 \qquad (52)$$

where $\vec{C}$ is a two dimensional velocity with axial and tangential components. Now, each flow parameter can be expressed as

$$C = \overline{C} + C' \qquad (53)$$

and

$$C' = \mathrm{Re}\left[\hat{C} e^{\alpha x + i(y/R)}\right] \qquad (54)$$

is a small perturbation about the mean. A homogeneous set of equations for eigenvalues is obtained by substituting for each flow variable and linearizing.

$$\begin{bmatrix}
\alpha\overline{\Delta}_R & i\overline{\Delta}_R/R & 0 & 0 & 0 & 0 & A & 0 & 0 \\
0 & 0 & \alpha\overline{\Delta}_S & i\overline{\Delta}_S/R & 0 & 0 & 0 & C & 0 \\
0 & 0 & 0 & 0 & D & E & -B & -B & 0 \\
A & 0 & 0 & 0 & 0 & 0 & 0 & 0 & \alpha \\
0 & A & 0 & 0 & 0 & 0 & 0 & 0 & i/R \\
0 & 0 & C & 0 & 0 & 0 & 0 & 0 & \alpha \\
0 & 0 & 0 & C & 0 & 0 & 0 & 0 & i/R \\
0 & 0 & 0 & 0 & B & 0 & 0 & 0 & \alpha \\
0 & 0 & 0 & 0 & 0 & B & 0 & 0 & i/R
\end{bmatrix}
\begin{bmatrix}
\hat{C}_x^a \\ \hat{C}_y^a \\ \hat{C}_x^c \\ \hat{C}_y^c \\ \hat{C}_x^b \\ \hat{C}_y^b \\ \hat{\Delta}_R \\ \hat{\Delta}_S \\ \hat{P}/\rho
\end{bmatrix} = 0 \qquad (55)$$

where $A = \alpha\overline{C}_x^a + i(\frac{\overline{C}_y^a}{R})$, $B = \alpha\overline{C}_x^b + i(\frac{\overline{C}_y^b}{R})$, $C = \alpha\overline{C}_x^c + i(\frac{\overline{C}_y^c}{R})$,

$D = \alpha(H - \overline{\Delta}_R - \overline{\Delta}_S)$, $E = i(H - \overline{\Delta}_R - \overline{\Delta}_S)/R$

Then, the non-trivial homogeneous solution is

$$\left(\hat{C}_x^a, \hat{C}_x^a, \hat{C}_x^b, \hat{C}_x^b, \hat{C}_x^c, \hat{C}_x^c, \hat{\Delta}_R, \hat{\Delta}_S, \frac{\hat{P}}{\rho}\right) = \sum_{i=1}^{8} \hat{K}_i E_i \qquad (56)$$

where E_i 's are eigenvectors, and the complex constants $\hat{K}_i$'s are to be determined from matching.

2. 3. 3. The Upstream – Downstream Coupling

To connect upstream and downstream flows, the results from the blade scale analysis are used. According to the blade scale analysis, the flow variables depend on the local nondimentional tip clearances, t_R/H & t_S/H, and axial velocity, Φ. For example,

$$\frac{C_{x4}^a}{U} = \frac{C_{x4}^a}{U}\left(\frac{t_R}{H}, \frac{t_s}{H}, \Phi\right) \qquad (57)$$

The downstream and upstream perturbation quantities are determined from the blade scale results as shown below. The axisymmetric blade scale results on the right side of Eq. (58) are perturbed to account for the given geometric non-axisymmetry. The perturbation solutions then become non-axisymmetric radius scale results on the left side of Eq. (58). The local flow coefficient, Φ, is also determined from matching upstream and downstream flows.

Radius Scale Blade Scale

$$\begin{pmatrix} \hat{C}_x^a \\ \hat{C}_x^b \\ \hat{C}_x^c \\ \hat{C}_y^a \\ \hat{C}_y^b \\ \hat{C}_y^c \\ \hat{\Delta}_R \\ \hat{\Delta}_S \\ \hat{\underline{p}} \\ \rho \end{pmatrix}_{x=0+} = \left[\hat{\Phi}\frac{\partial}{\partial \Phi} + \left(\frac{e}{H}\right)_R \frac{\partial}{\partial(\frac{t_R}{H})} + \left(\frac{e}{H}\right)_S \frac{\partial}{\partial(\frac{t_S}{H})} \right] \begin{pmatrix} C_x^a \\ C_x^b \\ C_x^c \\ C_y^a \\ C_y^b \\ C_y^c \\ \Delta_R \\ \Delta_S \\ \underline{P} \\ \rho \end{pmatrix}$$

Perturbation

$$= \sum_{i=1}^{8} K_i \{E_i\} \qquad (58)$$

2. 4. Calculation of Rotordynamic Coefficients

From the perturbations in flow variables, rotordynamic excitation forces can be predicted. The tangential force exerted on the compressor by the fluid per azimuthal length is defined as

$$f_y = \lambda_R q(C_{y1} - C_{y2}^a) + \lambda_R q(C_{y1} - C_{y2}^a) + (1-\lambda_R - \lambda_R) q(C_{y1} - C_{y2}^b) \qquad (59)$$

where q is the local mass flux. The mean and the perturbation of f_y are, respectively

$$\bar{f}_y = \bar{\lambda}_R \bar{q}(\bar{C}_{y1} - \bar{C}_{y2}^a) + (1-\bar{\lambda}_R)\bar{q}(\bar{C}_{y1} - \bar{C}_{y2}^b) \qquad (60)$$

$$f_y' = \bar{\lambda}_R \bar{q}(\bar{C}_{y1} - \bar{C}_{y2}^a)\left[\frac{\lambda_R'}{\bar{\lambda}_R} + \frac{q'}{\bar{q}} + \frac{C_{y1}' - C_{y2}^a}{\bar{C}_{y1} - \bar{C}_{y2}^a}\right] + (1-\bar{\lambda}_R)\bar{q}(\bar{C}_{y1} - \bar{C}_{y2}^b)\left[\frac{-\lambda_R'}{1-\bar{\lambda}_R} + \frac{q'}{\bar{q}} + \frac{C_{y1}' - C_{y2}^b}{\bar{C}_{y1} - \bar{C}_{y2}^b}\right] \qquad (61)$$

The perturbation in f_y is almost like the torque variation envisioned by Thomas and Alford. However, they assumed that the flow remains axisymmetric upstream and downstream of the compressor, and, thus, ignored the effects of mass flux perturbation, $q'/\bar{q}$. However, as Eq. (48) shows, rotor and stator tip clearances do indeed induce azimuthal flow redistribution, and this flow redistribution results in a non-axisymmetric pressure distribution.

The pressure acting on the rotor hub is approximated as the average of pressures at the inlet and the exit of the rotor, $< P >$.

$$\langle P \rangle = \frac{P_1 + P_2}{2} = P_1 - \frac{P_1 - P_2}{2} = P_1 - \frac{1}{2}\frac{\rho}{2}[(C_{x2}^b)^2 \tan^2 \beta_2 - (U - C_{y1})^2] \qquad (62)$$

$$\langle P \rangle' = P_1' - \frac{\rho}{2}\left[\bar{C}_{x2}^b C_{x2}^b \tan^2 \beta_2 + (U - \bar{C}_{y1})C_{y1}'\right] \qquad (63)$$

Non-uniform tangential force and non-uniform pressure can thus be obtained from Eqs. (61) and (63). Upon projection onto the X, Y axes, the total excitation force coefficients, or the rotordynamic stiffness coefficients, are

$$(\alpha_Y + i\alpha_X)_{(total)} = \frac{-\hat{f}_y + iL < \hat{P} >}{\left|\bar{f}_y (e/H)\right|} \qquad (64)$$

The total coefficients $\alpha_{(total)}$ are composed of contributions from tangential force asymmetry $\alpha_{(wd)}$ and pressure asymmetry $\alpha_{(p)}$. Forces along the rotor offset are called direct forces and are denoted with a subscript X. Forces perpendicular to the rotor offset are called cross forces and are denoted with a subscript Y.

3. Model Predictions

This section presents the model predictions for the selected baseline compressor and other compressors. Initially, the "baseline" compressor chosen for this study is explained, and the predictions for this compressor are given in the following order. First, the radial flow redistribution induced by axisymmetric rotor and stator tip clearances is presented. Second, the azimuthal flow redistribution due to non-axisymmetric tip clearances is shown. For both, differences and similarities between the predictions of the new model with rotor and stator clearances (RSC model) and those of the model with only the rotor clearance (RC model) (Park, 1998) are brought out. Third, rotordynamic coefficients at the design point and off-design points are discussed. Finally, the effects of various compressor designs on rotordynamic stiffness coefficients are presented.

The characteristics of the "baseline" compressor are given in Table 1. The design flow coefficient, reaction, and work coefficient have all been set to 0.5 because they are representative of modern compressors. The tip clearance values of 2% of the annulus height have been selected because such value is common in research experiments.

Parameter	Value
Φ_D	0.50
Ψ_D	0.50
R_D	0.50
$\bar{t}_R/H$	0.02
$\bar{t}_S/H$	0.02

Table 1: Baseline compressor specifications at the design point.

3.1 Blade Scale Predictions

Figure 5 shows the radial profiles axial velocity, tangential velocity, and yaw angle at the rotor exit after the flow has split into two streams. The hub and endwall are at $z/H = 0.0$ and $z/H = 1.0$, respectively. Stream "a" is retarded in the axial direction and underturned in the tangential direction relative to Stream "b". Figure 6 shows the same type of profiles at the stator exit. Now, the flow has split into three streams. Relative to Stream "b", which goes through both rotor and stator blades, Stream "c" shows characteristics similar to those of Stream "a". Such results agree with the corresponding predictions from the RC model of Park (1998) shown in Figures 7 and 8. Underturning is due to the effects of the tip leakage flow. The axial momentum defect is caused by flow migration away from the tip clearance where the pressure rise across the compressor stage is sensed more. Such effects increase with increasing tip clearance, and this trend agrees with the experimental findings of Hunter & Cumpsty (1982).

Comparing Figures 6 and 8, the obvious difference between the new RSC model and the RC model is Stream "c" which does not exist in Figure 8. Thus, the new model can incorporate the effects of stator gap on the flow field. Focusing on Stream "a", the stream's mass fraction, degree of axial momentum defect and underturning in Figures 6 and 8 are virtually identical. This is because the downstream stator tip clearance effect occurs over a length scale on the order of the tip clearance. However, the axial blade spacing is on the order of the blade chord which is at least a couple of orders of magnitude larger than the tip clearance. Thus, Streams "a" and "c" are practically decoupled from each other.

3. 2. Radius Scale Predictions

3. 2. 1. Azimuthal Flow Redistribution

First, the upstream azimuthal flow redistribution induced by tip clearance asymmetry is discussed. Nondimensional velocity and pressure perturbations upstream of the compressor predicted by the RC model and the new RSC model are plotted versus azimuthal location θ in Figure 9 and 10, respectively. The minimum gap is at $\theta = 0^\circ$ and maximum gap is at $\theta = 180^\circ$. Roughly, the mass flux is higher near the minimum gap in both cases. Again, the higher downstream pressure is "felt" more near the maximum gap ($\theta = 180^\circ$). The result is a tangential flow migration away from the larger gap towards the smaller gap. Then from the Bernoulli relation, the pressure decreases as flow accelerates. The magnitudes of both perturbations increase significantly when the stator clearance is introduced. As Eq. (58) shows, the clearance asymmetry acts as the forcing term which induces azimuthal flow redistribution. Therefore, imposing stator tip clearance asymmetry in addition to the rotor tip clearance asymmetry strengthens the forcing effect. Thus, the flow becomes more non-uniform with rotor and stator tip clearances.

Next, the rotordynamic consequences of such flow redistribution are presented. Tangential force perturbation (also referred to as the torque asymmetry or blade loading variation) is plotted versus θ in Figure 11. Since the force on the compressor by the fluid acts in a direction opposite to the direction of rotation, the mean value of tangential force, $\bar{f}_y / \dot{m}U$, is negative. Therefore, according to Figure 11, the compressor rotor blade is loaded less near the maximum gap. The unloading near the maximum gap occurs mainly because the tip leakage flow rate is higher there. Such prediction has been verified by the experimental data from the GE LSRC (Ehrich et al, 2000). Also, introducing stator clearance asymmetry hardly changes the perturbation in blade loading because the rotor tip leakage flow is practically decoupled from the stator tip clearance.

The perturbation in the rotor region static pressure is plotted versus θ in Figure 12. The pressure has its maximum near the maximum gap($\theta = 180^\circ$). Although a similar trend is suggested by the GE's LSRC data, the corresponding experimental data do not exist yet to confirm this effect in compressors. Unlike the blade loading perturbation, the pressure perturbation is more sensitive to the addition of stator clearance asymmetry (Figure 10). In turbines, the pressure asymmetry, predicted by a similar actuator disc model, matched well with experimental data (Song & Martinez-Sanchez, 1997b).

3. 2. 2. Design Point Rotordynamic coefficients

The predicted excitation coefficients from the new RSC model are listed in Table 2 and those from the RC model are given in Table 3. The coefficients due to blade loading variation are $\alpha_{(wd)}$'s and those due to pressure variation are $\alpha_{(p)}$'s. Both models predict the following. The blade loading variation induces a negative cross force, which promotes a backward whirl, and a negligible direct force. The pressure effect leads to a positive cross force, which induces a forward whirl, and a positive direct force. However, the models predict different total coefficients. The new model predicts that the $\alpha_{Y(total)}$ is positive because $\alpha_{Y(p)}$ is bigger than $\alpha_{Y(wd)}$. Thus, a net positive cross force is predicted. However, the RC model predicts a negligible cross force because the blade loading and pressure effects cancel each other out in Y direction. Both models predict a positive $\alpha_{X(total)}$ between 0.4 and 0.6.

In comparison, the parallel compressor model of Ehrich (1993) can predict only $\alpha_{Y(wd)}$. The model uses the difference between compressor characteristics at different axisymmetric tip clearances to predict torque asymmetry which is assumed to be in phase with the clearance distribution. However, no pressure information is available for the parallel compressor model to predict pressure asymmetry. Nevertheless, like the new RSC model, the parallel compressor model predicts a negative cross force due torque asymmetry.

Direction	$\alpha_{(wd)}$	$\alpha_{(p)}$	$\alpha_{(total)}$
X	0	+0.4	+0.4
Y	-0.7	+2.1	+1.4

Table 2: Excitation force coefficients for the baseline compressor ($\Phi_D = 0.50, \Psi_D = 0.50, R_D = 0.50$) predicted from the new model (RSC).

Direction	$\alpha_{(wd)}$	$\alpha_{(p)}$	$\alpha_{(total)}$
X	0	+0.6	+0.4
Y	-0.7	+0.6	-0.1

Table 3: Excitation force coefficients for the baseline compressor ($\Phi_D = 0.50, \Psi_D = 0.50, R_D = 0.50$) predicted from the rotor clearance-only (RC) model of Park (1998).

3. 2. 3. Off-Design Point Rotordynamic Coefficients

Figure 13 shows a graph of excitation force coefficients versus the operating flow coefficient. In this case, to model an embedded stage, the IGV has been replaced with a stator row. If a compressor operates below its design flow coefficient, excitation force coefficients increase in magnitude because the amplitudes of flow perturbations are magnified at low $\overline{\Phi}$. These trends are similar to those predicted and measured in turbines (Song & Martinez-Sanchez (1997b)). Figure 14 shows a graph of the cross force excitation coefficient due to blade loading variation, $\alpha_{Y(wd)}$, plotted versus $\overline{\Phi}$. $\alpha_{Y(wd)}$ remains negative but decreases slightly in magnitude as $\overline{\Phi}$ increases. This trend has been verified experimentally in the LSRC at General Electric (Ehrich et al., 2000).

3. 3. Parametric Analysis Predictions

This section presents the predicted effects of compressor design parameters on the excitation force coefficients. The selected parameters are the design flow coefficient, Φ_D, the design work coefficient, ψ_D, and the design reaction, R_D. They determine compressor blade angles as shown below.

$$R_D = \frac{1}{2} - \left(\frac{\tan\alpha_1 - \tan\beta_2}{2} \right) \Phi_D \qquad (65)$$

$$\psi_D = 1 - \Phi_D (\tan\alpha_1 + \tan\beta_2) \qquad (66)$$

Thus, a change in the value of one of the parameters changes both rotor and stator blade shapes (i.e. angles), and the effects of various compressor designs can be examined. For parametric analysis, one of the three variables is changed while the other two are held constant at the "baseline" values.

Figure 15 shows variation of $\alpha_{(total)}$ and $\alpha_{(p)}$ as the design flow coefficient is increased. $\alpha_{(wd)}$ is the difference between $\alpha_{(total)}$ and $\alpha_{(p)}$. For the cross force, $\alpha_{Y(total)}$ decreases with increasing Φ_D primarily because $\alpha_{Y(p)}$ decreases as the magnitude of azimuthal flow non-uniformity is decreased. Also, $\alpha_{Y(wd)}$ remains negative and its magnitude increases with Φ_D. For the direct force, $\alpha_{X(p)}$ dominates over $\alpha_{X(wd)}$ and changes sign as the phase of pressure non-uniformity relative to tip clearance distribution shifts. These trends are similar to those predicted for turbines in Song & Martinez-Sanchez (1997b).

Figures 16 shows variation of excitation force coefficients as the design work coefficient is increased. In the Y direction, $\alpha_{Y(total)}$ increases primarily because $\alpha_{Y(p)}$ increases in magnitude. In the X direction, $\alpha_{X(total)}$ does not change much while $\alpha_{X(wd)}$ increases. Overall, increasing the work coefficient is equivalent to strengthening the intensity of discontinuity across the actuator disc. Thus, for a given imposed tip clearance asymmetry, the perturbations in the flow field increase. In addition, the phases of the flow perturbations relative to the clearance distribution also shift.

Figure 17 shows the variation of excitation force coefficients versus the design reaction. As R_D increases, $\alpha_{X(p)}$ does not change much, but $\alpha_{Y(p)}$ is reduced significantly. This change is due to the decrease in the magnitude of azimuthal flow non-axisymmetry. $\alpha_{(wd)}$ is relatively insensitive to R_D. Thus, at low design reactions, $\alpha_{Y(total)}$ is increased.

4. Conclusions

The new conclusions of this study can be summarized as follows.

1) A new analytical model has been developed to examine the effects of non-axisymmetry in rotor and stator tip clearances on the compressor flow field.
2) The new model has reconfirmed the following previously found trends – a)radial flow migration away from the tip clearance; b) azimuthal flow migration towards smaller gap area; and c) direction of rotordynamic forces which arise due to pressure and torque (i.e. blade loading) asymmetry.

In addition, for the baseline compressor, the following conclusions can be drawn.

3) Direct force is mostly due to the pressure asymmetry and is positive.
4) Torque asymmetry results in a negative cross force which, without damping, would promote a backward whirl. However, pressure asymmetry results in a positive cross force which would promote a forward whirl. The net result is a positive cross force.
5) The dominance of pressure asymmetry effects over those of blade loading asymmetry is due to the introduction of stator clearance asymmetry.
6) The flow associated with the rotor tip clearance is hardly affected by the existence of the downstream stator tip clearance.
7) The pressure asymmetry induced by azimuthal flow

redistribution increases significantly in magnitude with the addition of stator tip clearance asymmetry.

8) Operating at below the design flow coefficient increases the magnitude of excitation force coefficients.

Finally, from the results of parametric variation about the baseline compressor, the following conclusions can be drawn.

9) High design flow coefficient and high design reaction decrease the magnitudes of excitation force coefficients.
10) High design work coefficient increase the excitation force coefficients' magnitudes.

Acknowledgement

The financial support for this study has been provided by the Seoul National University Research Fund and the Turbomachinery and Power Machinery Research Center. Also, the authors have benefitted from constructive discussions with Professor Martinez-Sanchez of MIT.

References

1) Alford, J., 1965, "Protecting Turbomachinery from Self-Excited Rotor Whirl," ASME Journal of Engineering for Power, pp.333-334.
2) Chen, G. T., 1991, "Vortical Structures in Turbomachinery Tip Clearance Flows," Ph.D. Thesis, Department of Aeronautics and Astronautics, M.I.T..
3) Colding-Jorgensen, J. , 1992, "Prediction of Rotordynamic Destabilizing Forces in Axial Flow Compressors," ASME Journal of Fluids Engineering, Vol.114, pp.621-625.
4) Ehrich, F.F., 1993, "Rotor Whirl Forces Induced by the Tip Clearance Effect in Axial Flow Compressor," Journal of Vibration and Acoustics, Vol. 115, No.3, pp.509-515.
5) Ehrich, F.F., et al., 2000, "Unsteady Flow and Whirl-Inducing Forces in Axial-Flow Compressors; Part 2 – Analysis," ASME/IGTI TurboExpo 2000, Munich, Germany.
6) Graf, M.B., Wong, T.S., Greitzer, E.M., Marble, F.E., Tan, E.S., Shin, H.W., Wisler, D.C. , 1998, "Effects of Nonaxisymmetric Tip Clearance on Axial Compressor Performance and Stability," ASME Journal of Turbomachinery, Vol. 120, No. 4, pp. 648-661.
7) Horlock , J.H., and Greitzer, E. M. , 1983, "Non-Uniform Flows in Axial Compressors Due to tip Clearance Variation," Proceedings of the Institution of Mechanical Engineers, Vol. 197C, pp.173-178.
8) Hunter, I.H., and Cumpsty, N.A., 1982, "Casing Wall Boundary-Layer Development Through an Isolated Compressor Rotor," ASME Journal of Engineering for Power, Vol.104, pp. 805-818.
9) Martinez-Sanchez, M., and Gauthier, R. P., 1990, "Blade Scale Effects of Tip Leakage," Gas Turbine Laboratory Report #202, M.I.T..
10) Martinez-Sanchez, M., Jaroux, B., Song, S. J., and Yoo, S., 1995, "Measurement of Turbine Blade-Tip Rotordynamic Excitation Forces," Journal of Turbomachinery, Vol.117, July 1995, pp.384-393.
11) Park, K.Y. , 1998, "Non-uniform Compressor Flow Fields Induced by Non-axisymmetric Tip Clearance", M.S. Thesis, Department of Aerospace Engineering, Inha Univ. Korea.
12) Roh. H.Y. , 1997, "Blade Scale Effects of Tip Leakage Flow in Axial Compressors", B.S. Thesis, Department of Aerospace Engineering, Inha Univ., Korea.
13) Song, S.J., Martinez-Sanchez, M. , 1997, "Rotordynamic Forces due to Turbine Tip Leakage:Part 1- Blade Scale Effects," ASME Journal of Turbomachinery, Vol. 119, pp.695-703.
14) Song, S.J., Martinez-Sanchez, M. , 1997, "Rotordynamic Forces due to Turbine Tip Leakage:Part 2- Radius Scale Effects and Experimental Verification," ASME Journal of Turbomachinery, Vol. 119, pp.704-713.
15) Storace, A., et al., 2000, "Unsteady Flow and Whirl-Inducing Forces in Axial-Flow Compressors; Part 1 – Experiment," ASME/IGTI TurboExpo 2000, Munich, Germany.
16) Thomas, H.J., 1958, "Unstable Natural Vibration of Turbine Rotors Induced by the Clearance Flow in Glands and Blading," Bull. de l'A.I.M., Vol. 71, No. 11/12, pp.1039-1063.
17) Urlichs, K., 1983, "Clearance Flow Generated Transverse Forces at the Rotors of Thermal Turbomachines," NASA TM-77292.
18) Wohlrab, R., 1983, "Experimental Determination of Gap-Flow Conditioned Forces at Turbine Stages, and Their Effect on the Running Stability of Simple Rotors," NASA TM-77293.

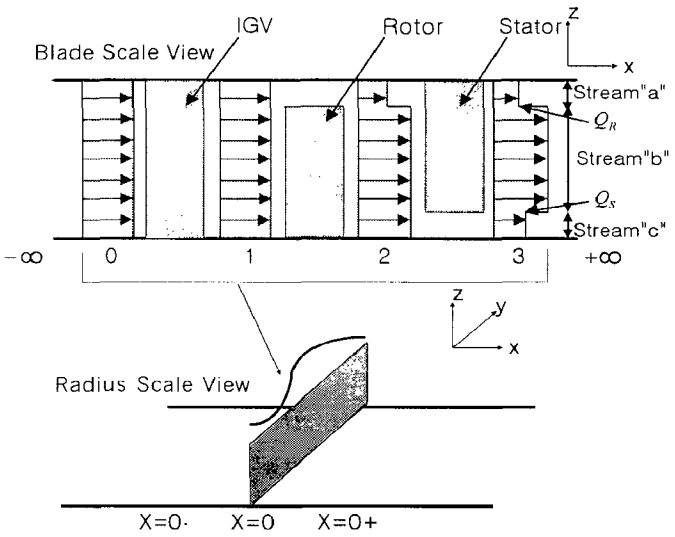

Figure 1: Blade and radius scale views of a compressor stage.

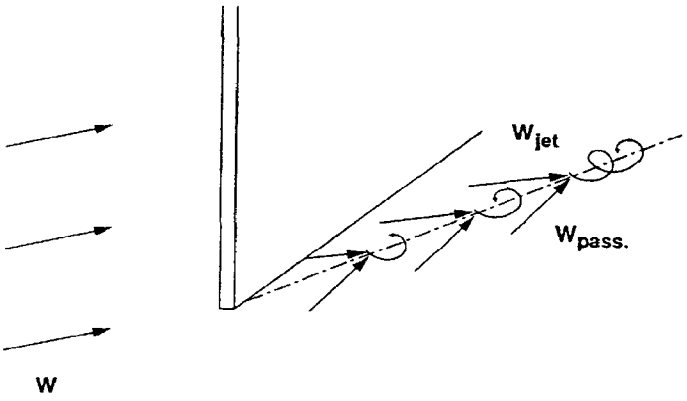

Figure 2: Schematic of the tip clearance flow model of Martinez-Sanchez (1990).

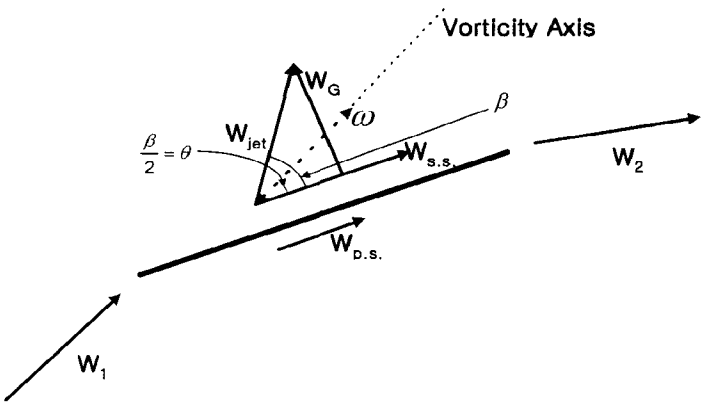

Figure 3: Geometry of compressor tip vortex roll up.

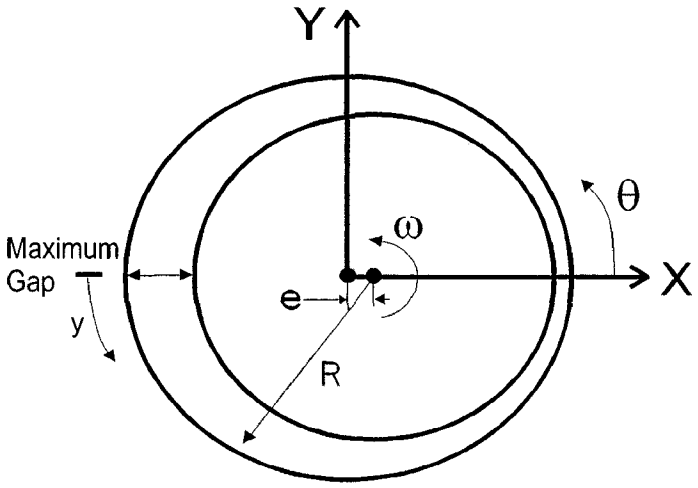

Figure 4: Coordinate system for the model.

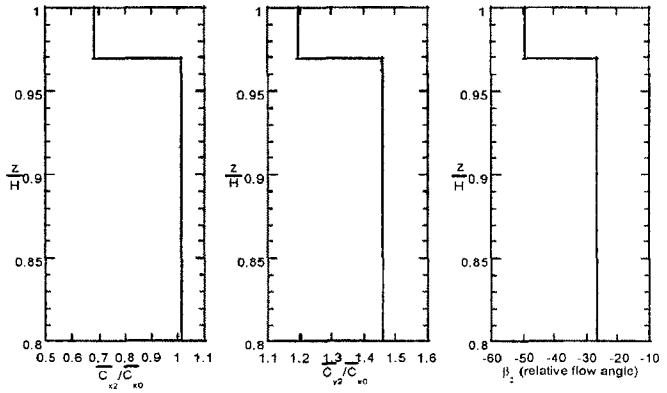

Figure 5: Radial distributions of axial velocity, tangential velocity, and yaw angle at rotor exit predicted by the new RSC model.

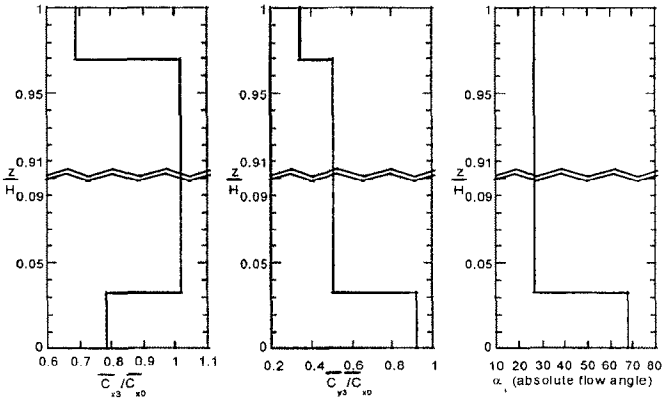

Figure 6: Radial distributions of axial velocity, tangential velocity, and yaw angle at stator exit predicted by the new RSC model.

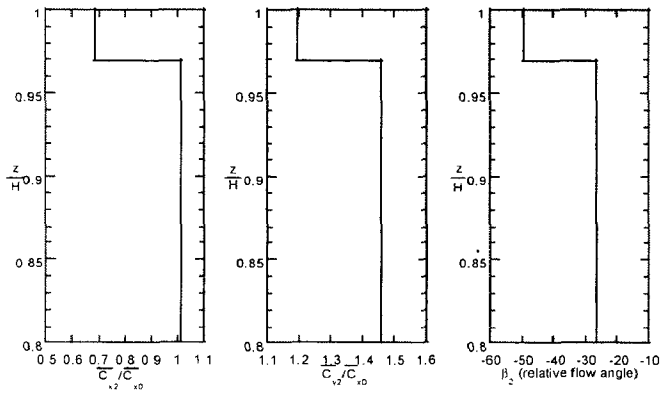

Figure 7: Radial distributions of axial velocity, tangential velocity, and yaw angle at rotor exit predicted by the RC model of Park (1998).

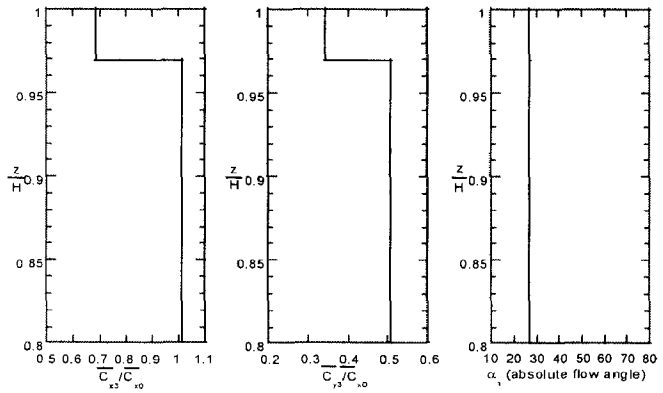

Figure 8: Radial distributions of axial velocity, tangential velocity, and yaw angle at stator exit predicted by the RC model of Park (1998).

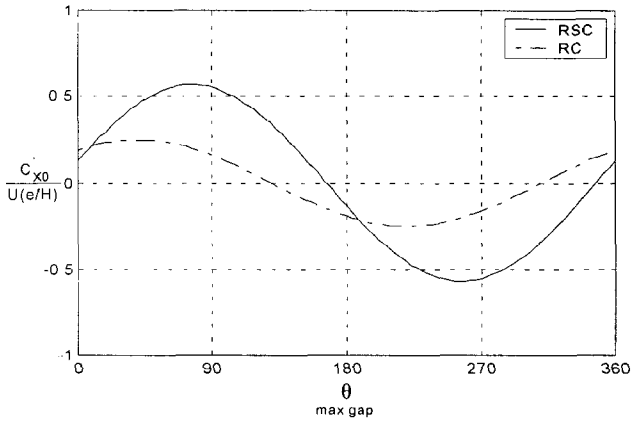

Figure 9: Upstream axial velocity perturbation vs. azimuthal angle.

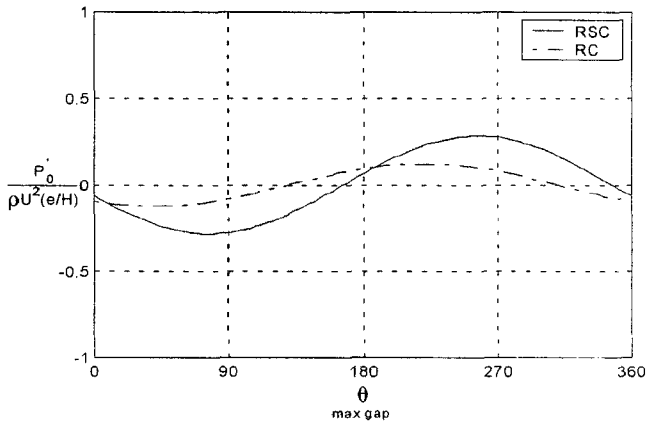

Figure 10: Upstream pressure perturbation vs. azimuthal angle.

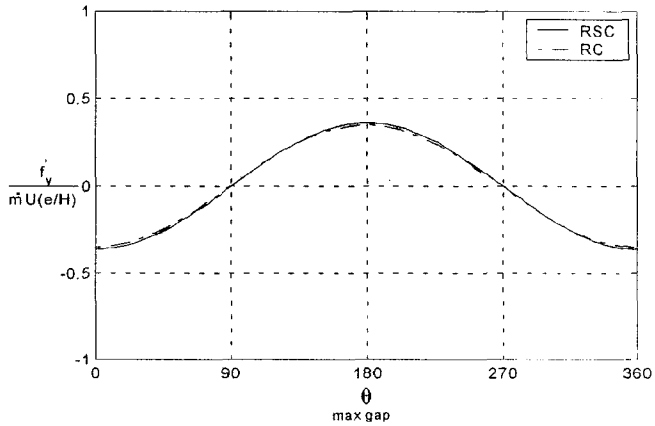

Figure 11: Rotor blade loading perturbation vs. azimuthal angle.

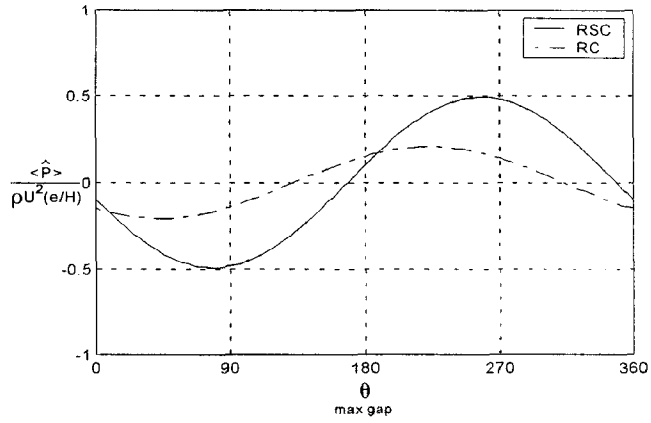

Figure 12: Perturbation in the average pressure on rotor hub vs. azimuthal angle.

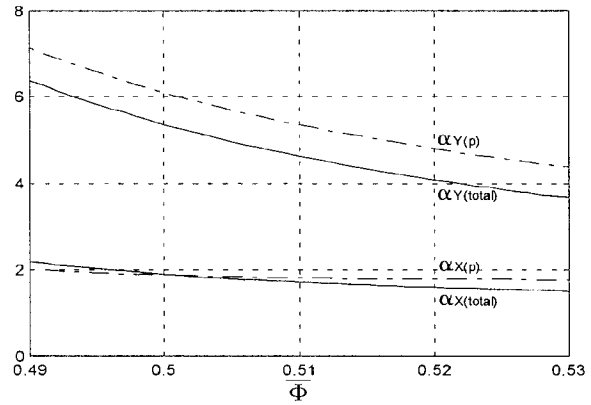

Figure 13: Predicted total and pressure rotordynamic coefficients vs. operating flow coefficient.

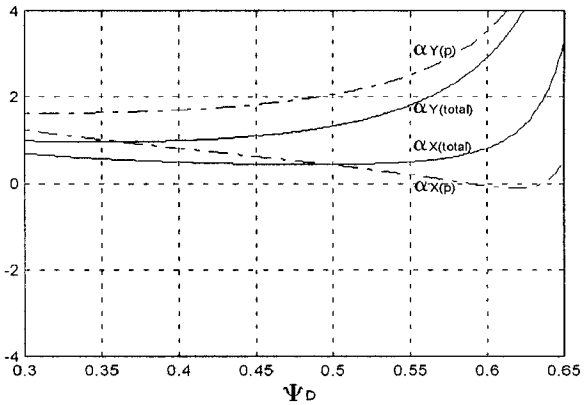

Figure 16: Predicted total and pressure rotordynamic coefficients vs. design work coefficient.

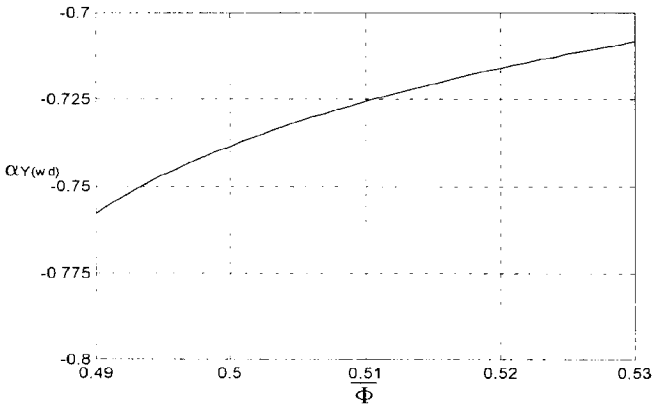

Figure 14: Predicted cross rotordynamic coefficients due to blade loading perturbation vs. operating flow coefficient.

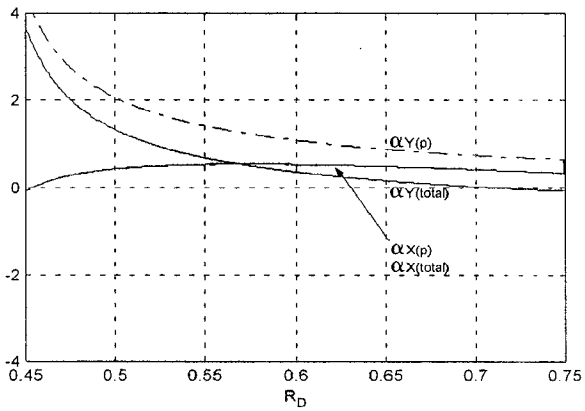

Figure 17: Predicted total and pressure rotordynamic coefficients vs. design reaction

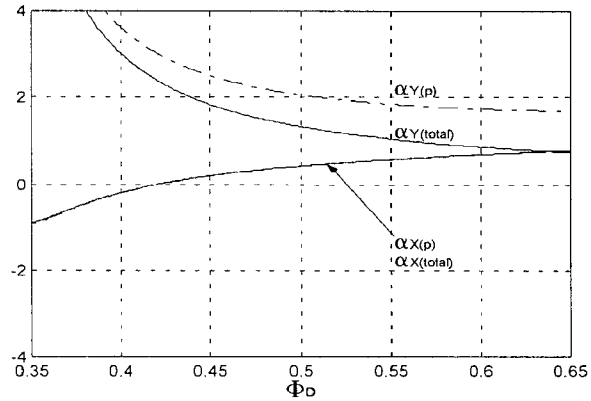

Figure 15: Predicted total and pressure rotordynamic coefficients vs. design flow coefficient.